^{55}Mn NMR study of quaternary half-metallic ferromagnetic $Co_2Mn_{1-x}Fe_xSi$ Heusler compounds

S. Wurmehl,[1,2,*] A. Alfonsov,[1] J. T. Kohlhepp,[3] H. J. M. Swagten,[3] B. Koopmans,[3] M. Wójcik,[4] B. Balke,[5] V. Ksenofontov,[5] C. G. F. Blum,[1] and B. Büchner[1,2]

[1]*IFW Dresden, Institute for Solid State Research, 01069 Dresden, Germany*

[2]*Institut für Festkörperphysik, Technische Universität Dresden, D-01062 Dresden, Germany*

[3]*Department of Applied Physics, Physics of Nanostructures, Eindhoven University of Technology, P.O. Box 513, 5600 MB Eindhoven, The Netherlands*

[4]*Institute of Physics, Polish Academy of Sciences, Aleja Lotnikow 32/46, 02-668 Warszawa, Poland*

[5]*Institut für Anorganische und Analytische Chemie, Johannes Gutenberg - Universität, 55099 Mainz, Germany*

(Received 30 August 2012; revised manuscript received 23 August 2013; published 25 October 2013)

In this work, the ^{55}Mn spin-echo nuclear magnetic resonance technique is used to systematically analyze the complete substitutional series $Co_2Mn_{1-x}Fe_xSi$ in terms of the resonance frequencies of the satellite structure and the corresponding hyperfine fields of the ^{55}Mn nuclei. The frequency spacing between satellite lines is constant within a compound, but decreases with increasing Fe concentration x, which originates in changes in the band structure. These changes are also responsible for the altered resonance frequencies observed for the same third shell environment but corresponding to a different overall Fe concentration x. All modifications in the hyperfine field upon substitution of Mn by Fe can be uniquely assigned to an entirely random distribution of Mn and Fe limited to only one (4*b*) out of four fcc sublattices constituting the $L2_1$ Heusler structure, demonstrating that the complete substitutional series $Co_2Mn_{1-x}Fe_xSi$ is crystallographically very well defined. This very high degree of order sets the stage for the observation of stable half-metallic ferromagnetism which is typically very sensitive to the structural order.

DOI: 10.1103/PhysRevB.88.134424 PACS number(s): 75.47.−m, 75.30.−m, 71.20.Be

I. INTRODUCTION

Half-metallic ferromagnets having a high stability of the minority band gap and, thus, a robust half-metallic behavior, are favored for spintronic applications.[1,2] If the Fermi energy is close to one of the edges, the band gap may easily be affected by disorder or by quasiparticle excitations.[1,2] Therefore, compounds with the Fermi energy located in the middle of the band gap are highly desirable.[1,2] A tunnel magnetoresistance device showing 832% TMR at 2 K and 386% at room temperature has been realized using the quaternary Heusler compound $Co_2FeAl_{0.5}Si_{0.5}$ as one example of such a robust half-metallic ferromagnet.[3] In addition, Shan *et al.* reported that this material exhibits half-metallic ferromagnetism even at room temperature.[4] Members of the substitutional series $Co_2Mn_{1-x}Fe_xSi$ with $x \sim 0.5$ are also predicted to exhibit this particular stable half-metallic behavior.[1,5] They belong to the class of X_2YZ Heusler compounds,[6] crystallizing in the $L2_1$ structure with the related space group $Fm\bar{3}m$.[7]

Several types of disorder were identified in Heusler compounds,[7] which have been also experimentally observed (see, e.g., Ref. 8 and references therein). The ordering in these different structure types have a high impact on the spin polarization, as some types of antisite disorder destroy half-metallic ferromagnetism,[9–12] requesting thorough structural characterization.

The structure of the complete substitutional series $Co_2Mn_{1-x}Fe_xSi$ was studied and verified to be $L2_1$ by combining several techniques such as x-ray diffraction, Mößbauer spectroscopy, extended x-ray absorbtion fine-structure measurements, high- and low-temperature magnetometry, and differential scanning calorimetry.[1,13,14] In addition to the predicted high spin polarization and high degree of order, the $Co_2Mn_{1-x}Fe_xSi$ series also offers very high Curie temperatures, namely 1100 K [Co_2FeSi (Ref. 13)] and 985 K [Co_2MnSi (Ref. 1)].

From a crystallographic point of view, the $L2_1$ structure type requires a random distribution of the Mn and Fe atoms on the 4*b* Wyckhoff position in the case of the quaternary compounds, whereas a complete preferential ordering would lead to a different structure type, symmetry, and space group.

Nuclear magnetic resonance (NMR) spectroscopy is able to distinguish between a preferential ordering and a random distribution of Mn and Fe in $Co_2Mn_{1-x}Fe_xSi$.[15–17] The NMR frequencies are strongly dependent on the local environment of the probed nuclei (^{55}Mn) which provides the possibility to resolve the occupation and local hyperfine fields of the nearest coordination shells of this atoms.[15,18–21] In some cases higher shell effects are visible as well.

In this paper, NMR was used to investigate the local environment of the complete substitutional series $Co_2Mn_{1-x}Fe_xSi$ and in particular to analyze the impact of the partial substitution on the ^{55}Mn hyperfine magnetic field (for experimental details see Ref. 22). By comparison of different structural models, the origin of the line splitting is identified as a random distribution of Mn and Fe in the third and higher shells. It is shown that the frequency spacing between adjacent resonance lines decreases with increasing Fe concentration x. This points to changes in the transferred hyperfine fields with increasing Fe concentration x, similarly to the observation of Wójcik *et al.* for $Co_2FeAl_{1-x}Si_x$.[23] The band-structure calculations,[1] predicting a very stable half-metallicity of the compounds with $x \approx 0.5$ were performed using a supercell with a preferential distribution of Fe and Mn. Thus, it might be quite relevant to recalculate the band structure of $Co_2Mn_{1-x}Fe_xSi$ including the experimentally verified random distribution of Mn and Fe, and to check whether the minority band gap and the half-metallicity is conserved. The high crystallographic order of all members

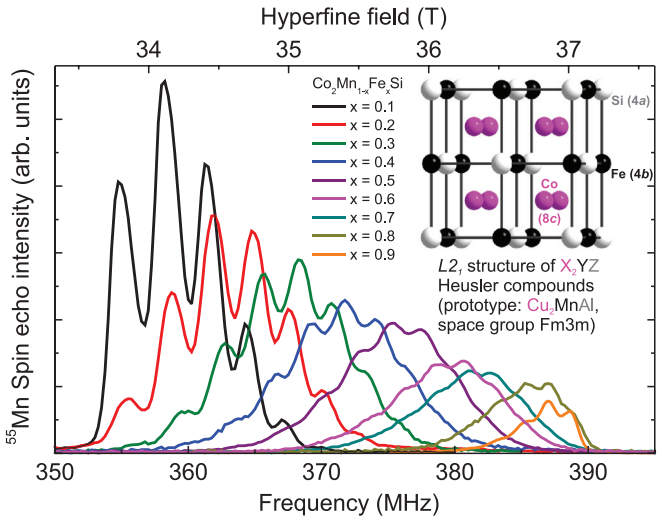

FIG. 1. (Color online) The ^{55}Mn spectra of all members of the substitutional series as a function of frequency (bottom axis) and as a function of the hyperfine field (top axis). The inset shows the Heusler crystal lattice in the $L2_1$ structure with the corresponding Wyckoff positions of the X, Y, and Z atoms.

of the substitutional series, demonstrated by the ^{55}Mn NMR results, sets stage for the half-metallic character and the high degree of spin polarization of $Co_2Mn_{1-x}Fe_xSi$ and illustrates that in particular the $Co_2Mn_{1-x}Fe_xSi$ compounds with $x \approx 0.5$ may be ideal candidates for spintronic applications.

II. RESULTS AND DISCUSSION

A. NMR spectra of the $Co_2Mn_{1-x}Fe_xSi$ substitutional series

The NMR experiments were performed on pieces of polycrystalline samples in an automated, coherent, phase sensitive spin-echo spectrometer at temperature $T = 4.2$ K,[24] and at zero external magnetic field. All NMR spectra were corrected for the magnetic enhancement factor as well as for the ν^2 dependence. For experimental details see Ref. 22.

Figure 1 shows the ^{55}Mn NMR spectra of all members of the substitutional series together with the Heusler crystal lattice ($L2_1$-type structure) and the corresponding Wyckoff positions of the X, Y, and Z atoms. Note that all spectra are scaled in order to better represent the increasing Fe content. Apparently, the spectra shift to higher resonance frequencies with increasing Fe content x. As can be seen, all spectra exhibit a splitting into resonance sublines (satellite lines). For further analysis the observed lines of all spectra were fitted using a sum of Gaussian lines (represented in Fig. 2 by thick solid lines). Note that the labels of the individual lines in Fig. 2 represent the Fe and Mn occupations in the third-neighbor shell of the ^{55}Mn nuclei, which determine the resonance frequency for a given surrounding, as will be discussed in Sec. II C. The width of these Gaussian lines were constrained to be identical within each compound. Figure 2 shows the ^{55}Mn spectra of $Co_2Mn_{0.1}Fe_{0.9}Si$ (a), $Co_2Mn_{0.3}Fe_{0.7}Si$ (b), $Co_2Mn_{0.7}Fe_{0.3}Si$ (c), and $Co_2Mn_{0.9}Fe_{0.1}Si$ (d) as representatives of the $Co_2Mn_{1-x}Fe_xSi$ substitutional series. It has been found that the frequency spacing between the satellites, within some experimental uncertainty, remains constant for

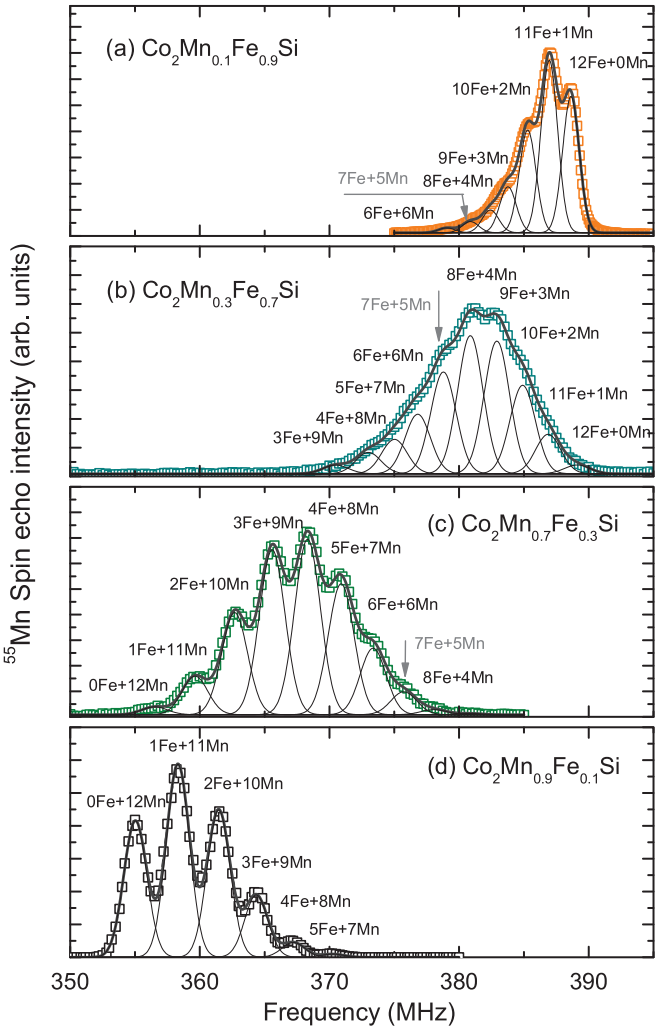

FIG. 2. (Color online) The figure exemplarily shows the spectra of $Co_2Mn_{0.1}Fe_{0.9}Si$ (a), $Co_2Mn_{0.3}Fe_{0.7}Si$ (b), $Co_2Mn_{0.7}Fe_{0.3}Si$ (c), and $Co_2Mn_{0.9}Fe_{0.1}Si$ (d), which demonstrate the splitting into multiplet structures with several resonance sublines. The Gaussian lines (thin solid lines) and the resulting fits (thick solid lines) are also given in (a)–(d). The arrows (grey) illustrate the shift of the resonance frequency for the 7 Fe + 5 Mn environment (grey) as a function of the nominal Fe concentration x.

each spectrum. However, this frequency spacing shows a pronounced dependence on the Fe concentration. The results of the analysis, such as mean spacing and mean satellite linewidth for a particular Fe concentration, are given in Table I.

The spectra of low Fe content compounds show better resolved lines, while the spectra of the compositions with medium and high Fe content have a more continuous shape with merging lines. Moreover, the number of observed lines increases from 6 lines ($Co_2Mn_{0.9}Fe_{0.1}Si$) to 11 lines ($Co_2Mn_{0.5}Fe_{0.5}Si$) with increasing Fe concentration x. At even higher x the number of lines decreases again to 7 lines for $Co_2Mn_{0.1}Fe_{0.9}Si$. Obviously, the mean spacing between adjacent satellite lines is larger for the Mn-rich than for the Fe-rich compounds (see Fig. 2 and Table I).

A comparison of the satellite linewidths of the complete substitutional series (see also Ref. 16) reveals that the linewidth Γ first increases with increasing Fe concentration x but

TABLE I. Mean spacing between adjacent lines, the mean width of the lines in the spectra of $Co_2Mn_{1-x}Fe_xSi$ and the mean absolute $|h_3|$ values calculated using Eq. (5).

x	Mean spacing (MHz)	Mean width (MHz)	Mean $\lvert h_3\rvert$ ($\times 10^6 \frac{A}{m\cdot\mu_B}$)
0.1	3.05 ± 0.08	1.78 ± 0.15	0.64 ± 0.02
0.2	2.93 ± 0.11	1.91 ± 0.08	0.64 ± 0.03
0.3	2.70 ± 0.10	1.99 ± 0.35	0.61 ± 0.02
0.4	2.66 ± 0.08	2.11 ± 0.06	0.62 ± 0.02
0.5	2.35 ± 0.07	2.19 ± 0.27	0.58 ± 0.02
0.6	2.19 ± 0.08	2.05 ± 1.35	0.55 ± 0.02
0.7	2.07 ± 0.20	1.95 ± 0.54	0.55 ± 0.02
0.8	1.59 ± 0.09	1.36 ± 0.20	0.43 ± 0.02
0.9	1.60 ± 0.09	1.28 ± 0.27	0.42 ± 0.02

eventually decreases after reaching a maximum (around 2 MHz at medium Fe concentration compounds). Interestingly, the linewidth of the Fe-rich compounds is even smaller than the linewidth of the Mn-rich compounds (see Sec. II H).

B. Contributions to the hyperfine field

The most dominant contribution to the effective field experienced by a nucleus in ferromagnetic materials is the hyperfine field term which for 3*d* metals mainly consists of contributions from the Fermi-contact field.[25] The Fermi-contact field is related to interactions of *s* electrons with the on-site magnetic moments mediated via the hyperfine coupling constants. Besides the contributions from the on-site magnetic moments, a significant contribution is the transferred contact field from the neighboring atoms which emerges from the polarization of the conduction *s* electrons by the magnetic moments of the surrounding atoms.[25–27] Bearing this in mind, pronounced differences in resonance frequencies consequently hint to pronounced differences in the magnetic environment of the NMR active atom. Apart from that, this term makes the hyperfine field sensitive to changes in the local crystallographic environment.[28,29] Please note that the coupling constants for the core and the transferred contributions to the contact field are related to the electronic structure of a system, which allows one to monitor changes in the electronic structure at least qualitatively by studying the evolution of the hyperfine fields, e.g., within a substitution series.[23] Therefore, the measurement of the hyperfine field gives the possibility to study the local magnetic, electronic, and structural surroundings of the NMR active atom.

C. Origin of the hyperfine field splitting

It is well known that antisite disorder, yielding different types of structure ($A2$, $B2$, or DO_3), affects the local hyperfine fields in clearly distinguishable ways. For example, the $A2$ type order yields a single, but very broad NMR line, which consists of many unresolved resonance lines corresponding to a large number of possibilities to distribute X, Y, and Z atoms on the 1*a* position of the $A2$ lattice. In the case of $A2$ ordered Co_2FeAl the ^{59}Co NMR linewidth amounts to a value of about ∼100 MHz (∼10 T).[27,30–32] The $B2$-type order (intermixing of Y and Z atoms) leads to a splitting of the resonance line to a set of sublines with a rather large spacing, due to pronounced differences in the magnetic moments between a transition metal and a main group element. In the case of Co_2MnSi the spacing, measured on ^{55}Mn nuclei, is about ∼50 MHz (∼5 T).[26] Similarly, in the case of Co_2FeAl, Y/Z mixing ($B2$-type order) leads to the splitting of the ^{59}Co lines with a spacing of about ∼30 MHz (∼3 T).[27,30–32] In addition, $B2$-type order in $Co_2Mn_{1-x}Fe_xAl$ yields only seven Mn/Fe sites with nonequivalent local hyperfine field, as it is shown in Ref. 33. The DO_3-type order (exchange of X and Y atoms) leads to a reduction of the hyperfine field at the Y atoms,[33–35] yielding a splitting into nine sublines.

As can be seen in Fig. 2, the number of well identified lines for $Co_2Mn_{1-x}Fe_xSi$ continuously changes from 6 to 11 and then back to 7 with increasing Fe content x. This fact together with experimentally observed line spacing (see Table I) rules out $A2$, $B2$, and DO_3 types of order in $Co_2Mn_{1-x}Fe_xSi$. In addition, the ^{59}Co NMR measurements performed on the same samples support the absence of $A2$, $B2$, and DO_3 types of order (^{59}Co NMR data were not included in this work).

Consequently, the line splitting is attributed to the $L2_1$ structure with a random distribution of Mn and Fe on the 4*b* position, leading to the existence of ^{55}Mn atoms with a varying number of Fe neighbors.[36] Every satellite line in the ^{55}Mn NMR spectra is attributed to a different number of Fe next neighbors in the third shell of the ^{55}Mn nuclei.[15] Assuming that Fe randomly substitutes for Mn, the probability to find a certain surrounding of the ^{55}Mn nuclei is given by the binomial distribution, represented by Eq. (1) (random atom model). In the present case, the probability to find n Mn and (12-n) Fe on the $N = 12$ positions of the third coordination shell of the ^{55}Mn nuclei in the $L2_1$ structure in a particular compound with the overall Fe concentration x is given by

$$P(n,x) = \frac{N!}{(N-n)!n!}(1-x)^{N-n}x^n. \quad (1)$$

D. Comparison of the binomial random atom model with the experimental data

In order to further confirm the random distribution of Mn and Fe for the complete substitutional series and to determine the real Fe concentration x, the relative areas of the resonance lines found experimentally are compared to the relative probabilities obtained by Eq. (1) (see Fig. 3). The determination of the real Fe concentration x was done by fitting the probability predicted by a binomial distribution [Eq. (1)] to the experimental data, having the Fe concentration x as a fit parameter. This optimization process was monitored by the least-square method (see Refs. 15 and 21 for details). For the comparison of the measured Fe concentration x with the nominal see Ref. 37.

The comparison of the experimental results with the binomial distribution curves explains the observation of less than 13 lines in all ^{55}Mn spectra, as the probabilities for some particular surroundings (e.g., 6 Fe + 6 Mn, 7 Fe + 5 Mn, etc., for $Co_2Mn_{0.9}Fe_{0.1}Si$, Fig. 2) are too low to be observed in the NMR experiment. This also explains the increase in the number of lines with increasing Fe concentration x and the decrease to 7 lines for $Co_2Mn_{0.1}Fe_{0.9}Si$ after a maximum of

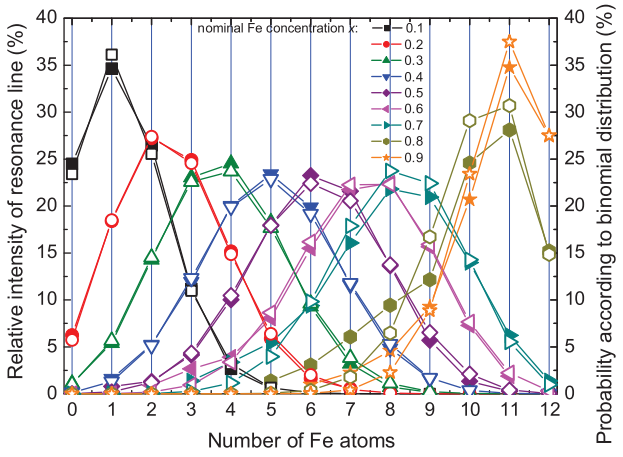

FIG. 3. (Color online) Relative areas of the resonance lines as a function of the number of Fe atoms in the third shell of ^{55}Mn. The full symbols represent the results obtained by fitting the experimental data with Gaussian lines, while the open symbols represent the probabilities as calculated using a binomial distribution of Fe on the 4*b* position. The lines are drawn to guide the eye.

11 lines ($Co_2Mn_{0.5}Fe_{0.5}Si$). The shape of all experimentally obtained distribution curves (Fig. 3, full symbols) follows the calculated binomial distribution (Fig. 3, open symbols). This confirms the predominantly random distribution of Fe and Mn on the 4*b* position for the complete substitutional series. Smaller deviations of the experimental data from the binomial distribution model are observed for the Fe-rich compounds with an Fe concentration $x \geqslant 0.7$, which is seen in Fig. 3. This is also apparent in the values for the overall sum of the least squares. On the other hand, all samples represent almost ideal stoichiometric $Co_2Mn_{1-x}Fe_xSi$ compounds.[37] Therefore, the difference between random atom model and experimental data is not related to the properties of a particular sample but is an intrinsic property of these compositions. This observation may point to a small tendency of Mn to separate in Co_2FeSi, leading to a not entirely homogenous distribution of Mn in the Fe-rich compounds. Apparently, Mn as a next neighbor is less favored than Fe in $Co_2Mn_{1-x}Fe_xSi$ with $x \geqslant 0.7$, which points to a higher tendency to built-up similar environments like in the pure Co_2FeSi.

E. Influence of the partial substitution of Mn by Fe on the hyperfine field

The probabilities to observe a particular neighboring environment can be directly compared to the intensities of a spin-echo NMR measurement.[26,27] The corresponding resonance frequencies are related to the hyperfine fields of the active atom in this certain environment as explained in the following.

The hyperfine field $H(Y^0)$ experienced by the Y^0 atom will depend on a particular environment and one expects that the effective hyperfine field at the atom Y^0 is composed of the on-site hyperfine field $H_0(Y^0)$ and the transferred hyperfine fields emerging from the magnetic moments of the surrounding atoms:[26]

$$H(Y^0) = H_0 + H_1 + H_2 + H_3 + \cdots = \sum H_i, \qquad (2)$$

where the indices are for the ith shell. In a simple model each contact hyperfine field term may be written as $h_i \sum m_{i,j}(I)$, where $m_{i,j}(I)$ is the moment of the jth atom $I = X$, Y, or Z in the ith shell. For the $X_2Y_{1-x}Y'_xZ$ compound this relates to

$$\begin{aligned} H(Y^0) = {} & H_0(Y) + 8h_1m(X) + 6h_2m(Z) + h_3[(12-n)m(Y) \\ & + nm(Y')] + 24h_4m(X) + 8h_5m(Z) \\ & + h_6[(6-n)m(Y) + nm(Y')] + \cdots \end{aligned} \qquad (3)$$

The terms with h_2 and h_5 are negligible as the Z element does not add to the magnetic moment. In order to focus on the analysis of the most important contributions to the hyperfine field $H(Y^0)$ experienced by the Y^0 atom, the contribution of coordination shells higher than the third shell can also be neglected in the first approximation, which simplifies Eq. (3) and leads to Eq. (4):

$$H(Y^0) = H_0(Y) + 8h_1m(X) + h_3[(12-n)m(Y) + nm(Y')]. \qquad (4)$$

According to Eq. (4), one expects a constant splitting of the resonance lines for a particular compound if one assumes that the magnetic moments and $H_0(Y)$ are not changed by an environment alteration.[26,38]

In line with this simple model, Fig. 4 demonstrates that the spacing between adjacent resonance lines can be regarded as nearly constant within each compound, with some experimental uncertainty (see spacing between vertical lines of symbols with each line corresponding to a certain compound). This supports the approximation that the local field $H_0(Y)$ and the magnetic moments of Co, Mn, and Fe are not changed by the partial substitution of Mn and Fe within a compound. In addition, the dependencies of the resonance frequencies assigned to a particular number of Fe neighbors for all spectra follow reasonably well the linear fits depicted as straight solid lines in Fig. 4. This linear dependence on the Fe concentration

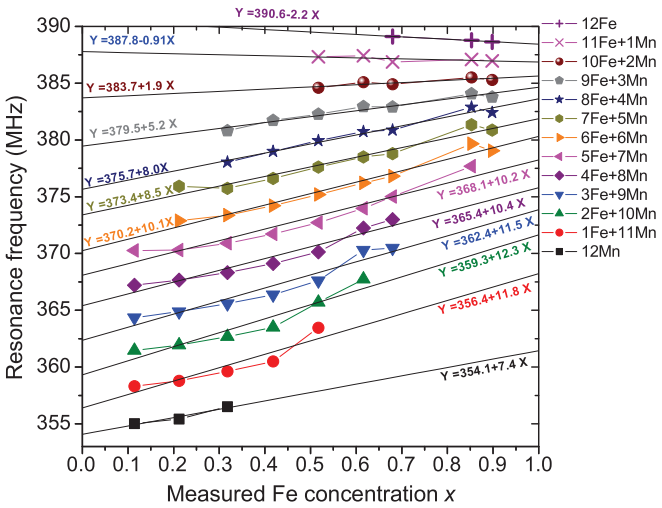

FIG. 4. (Color online) The resonance frequencies of the $Co_2Mn_{1-x}Fe_xSi$ alloys (measured at the ^{55}Mn atoms) as a function of the optimized Fe concentration x. Each symbol in Fig. 4 corresponds to a particular environment in the third shell of ^{55}Mn of a particular $Co_2Mn_{1-x}Fe_xSi$ alloy.

follows a similar trend as the value of the mean spacing within the corresponding compound.

Using Eq. (4) and assuming unalterability of the magnetic moments one can calculate the absolute difference between adjacent lines:

$$\Delta H(\mathrm{Mn}^0) = -h_3 m(\mathrm{Mn}) + h_3 m(\mathrm{Fe}) = -h_3[m(\mathrm{Mn}) - m(\mathrm{Fe})]. \quad (5)$$

According to calculations (see Ref. 1 for details), using a supercell and assuming a preferential order of Mn and Fe, only one magnetic moment for Mn and one for Fe, respectively, exists within a particular compound. This leads to mean values of the Co, Mn, and Fe magnetic moments within a particular compound. However, the small difference between the magnetic moments of Mn and Fe explains why H_0(Mn) stays nearly constant despite the alteration of the local environment, and why, thus, also the spacing between adjacent lines stays constant. Moreover, regarding the meaning of the terms in Eq. (4), one expects that the transferred hyperfine field at the ^{55}Mn nuclei for a particular compound is also constant for environments with different numbers of Mn and Fe in the third shell. Using Eq. (5) and the calculated magnetic moments, the absolute values of h_3 coefficients can be calculated (see Table I), assuming that the local hyperfine field due to the on-site Mn moment and the magnetic moments of Co, Mn, and Fe are not changed during the altering of the environment for a given compound.[26,38] In summary, according to our model, the constant difference in hyperfine field between the resonance lines within a compound is mainly related to the difference of the magnetic moments of Mn and Fe.

F. Transferred hyperfine field and band structure as a function of the overall Fe concentration x

Even though the spacing between adjacent resonance lines is approximately constant within each compound, it changes with increasing Fe concentration x in the substitutional series $Co_2Mn_{1-x}Fe_xSi$, as seen, e.g., from Table I. Figure 5(a) shows the calculated linear dependence of the Mn and Fe magnetic moments on the Fe concentration x. These values were calculated by the scalar relativistic full-potential linearized augmented plane wave–+U (FLAPW + U) method, as described in Ref. 1. Using these values, one can perform a linear regression in order to estimate all magnetic moments of Mn and Fe for all Fe concentrations x. This linear regression reveals that the difference between the magnetic moments of Mn and Fe is rather small with increasing concentration x while the satellite frequency spacing for a given Fe concentration is significantly decreasing [the gradient is −2.04 MHz/(Fe concentration x)] comparing all $Co_2Mn_{1-x}Fe_xSi$ compounds with increasing Fe concentration x, and that the mean spacing significantly decreases from $x = 0.1$ (3.05 ± 0.078 MHz) to $x = 0.9$ (1.60 ± 0.09 MHz). Apparently it is valid that $\Delta H(\mathrm{Mn}^0)_{\text{Mn -rich}} > \Delta H(\mathrm{Mn}^0)_{\text{Fe-rich}}$. Moreover, according to Figs. 4 and 5(b), this decrease is found to be linear as a function of the measured Fe concentration x.

In particular Heusler compounds with Mn on the Y position tend to have a high, localized magnetic moment[39,40] but they are also itinerant ferromagnets. This allows us to use a description based on a more local model to understand the spectra for a given Fe content x, however, we need to take their itinerant character into account to explain the change of spacing with increasing x.

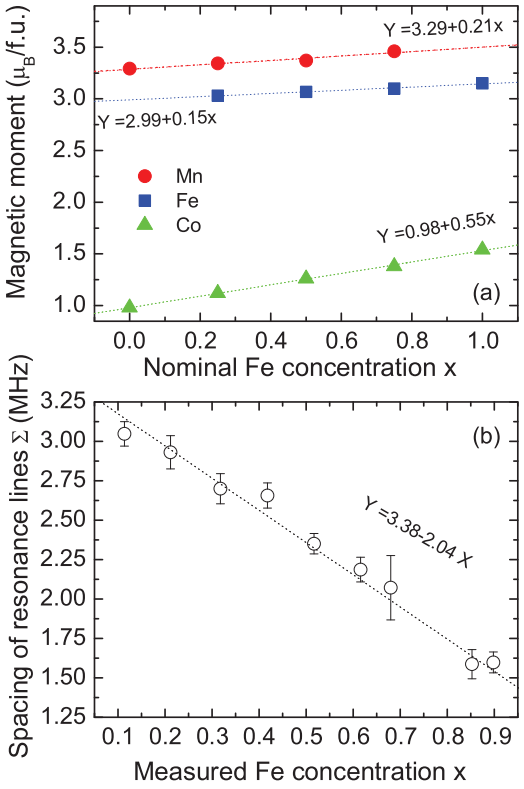

FIG. 5. (Color online) (a) The magnetic moments of Mn (full circles), Fe (full squares), and Co (full triangles) calculated using the FLAPW + U method, as described in Ref. 1. (b) The mean spacing Σ (open circles) as a function of the Fe concentration x, revealing that the spacing is the smallest for the Fe-rich compounds. The lines are drawn to guide the eye.

As was shown by Balke *et al.*,[1] with increase of the Fe concentration in $Co_2Mn_{1-x}Fe_xSi$, there are significant changes in the density of states. With increasing Fe content, different and/or additional bands may cross the s bands and hybridize with them. Hence, the observed alteration in the spacing reflects the changes in the density of states by adding additional electrons in different bands upon the substitution of Mn by Fe. Moreover, the fact that the resonance frequencies and the corresponding local fields show a different dependence upon substitution than the $Co_2FeAl_{1-x}Si_x$ series[23] may indicate a deviation from a rigid band shift upon substitution in $Co_2Mn_{1-x}Fe_xSi$. We will come back to the alteration of the electronic structure in Sec. II G.

G. NMR frequency shift

Additionally to the varying spacing, Fig. 4 also demonstrates that the resonance frequencies for a particular third shell environment slightly shift with increasing overall Fe content. Note that the frequency for a compound with Fe content $x = 0$ extrapolates to the value of 354.6 MHz, which is very close to the measured frequency in Co_2MnSi.[41] Each particular environment in the third shell of ^{55}Mn in a particular $Co_2Mn_{1-x}Fe_xSi$ composition is represented by a symbol in

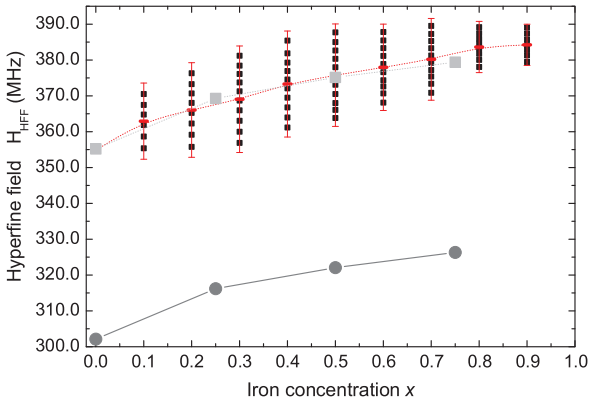

FIG. 6. (Color online) Shown are the H_{hf} of the measured resonance lines (black squares), the mean H_{hf} values of each compound, the width of their distribution (upright red lines) as well as calculated H_{hf} values using the FLAPW + U method (grey dots) as a function of the Fe concentration x. Additionally, the grey line with the grey squares represents the calculated H_{hf} values using the FLAPW + U method plus a constant term. This line shows that the general trend of the calculated hyperfine fields agrees well with the experimental ones and is different only by a constant shift.

Fig. 4. This shift is, additionally to Fig. 4, exemplarily also illustrated by the arrows in Fig. 1 for the 7 Fe + 5 Mn environment. Note that such a frequency shift is observed for all environments of the ^{55}Mn nuclei. As can be seen, in the case of the Mn-rich environments, the resonance frequencies strongly increase with increasing overall Fe concentration x, while the resonance frequencies of the very Fe-rich environments (about 11 or 12 Fe atoms in the third shell) decrease slightly with increasing x. This dependence is also monitored by the linear fits (black lines) in Fig. 4, revealing the gradients of the linear regressions. These gradients stay almost constant at about 10 MHz/(Fe concentration x) for the environments with less than 2 Mn neighbors and get smaller and even negative for the environments with 10, 11, and 12 Fe atoms. This observation is related to the "bending" of the hyperfine field dependence as a function of Fe content x (see Fig. 6), and is similar to the effect observed by Kawakami *et al.* in the $Co_2Mn_{1-x}Fe_xGa$ substitutional series.[42] In contrast, substitutional series without Fe, such as, e.g., $Co_2Cr_{1-x}Mn_xGa$, do not exhibit the bending of the lines, but a clear monotonic, linear behavior.[42] The fact that this bending is only observed for Fe-rich environments of various compounds is related to a different electronic structure for those compositions. The substitution of Mn by Fe in $Co_2Mn_{1-x}Fe_xSi$ leads to a gradual filling up of the s bands with electrons corresponding to the monotonous increase of the resonance frequency of the whole spectrum, which starts to "bend" at a certain x, when additional bands cross those s states or hybridize with them. The changes in the electronic structure manifest in changes in the hyperfine field, specifically the contact hyperfine field which is related to interactions of s electrons with the on-site magnetic moments, via the hyperfine coupling constants.[28] A recent study of the $Co_2FeAl_{1-x}Si_x$ Heusler compounds,[23] where there is no substitution of the magnetic Y atom, showed that electron doping has a global effect on the electronic structure and on the hyperfine field. Interestingly, the effect of bending is also observed in this material, but it is much less pronounced. This might be interpreted in terms of a rigid-band shift (compare Ref. 23) in the $Co_2FeAl_{1-x}Si_x$ series upon the substitution of Al by Si and a more complex change in the density of states when there is a replacement of one magnetic Y atom with another as is the case in $Co_2Mn_{1-x}Fe_xSi$. Taking into account the stronger localization of 3d electrons in the Mn-based Heusler compounds than in the Fe-based ones,[39,40] the bending might also reflect the transitions from a more localized (Co_2MnSi) to a more itinerant (Co_2FeSi) electronic structure.

There may be an additional contribution to the shift of the satellite lines due to the change of the Co magnetic moment with increasing Fe content [see Fig. 5(a)]. According to Eq. (4), the first shell consisting of eight Co nearest neighbors adds to the transferred hyperfine field at the measured ^{55}Mn nucleus. The impact of the Co atoms on this transferred hyperfine field scales with their magnetic moment, and therefore may contribute to the observed shift of the lines.

The bending of the hyperfine fields is also found in calculations using the FLAPW + U method, as described in Ref. 1. The calculated hyperfine fields are derived using a supercell to model the structure upon substitution of Mn by Fe; hence, the calculated hyperfine fields represent a mean value of all hyperfine fields for all different environments which are found in the real material due to the random distribution. Figure 6 compares the calculated H_{hf} values (grey dots) with the measured (black squares).

The measured hyperfine fields are represented by the maxima of the resonance lines. The mean H_{hf} values (red bars), corresponding to the arithmetic average of the highest and lowest frequency of the corresponding sublines of each spectrum, as well as the overall width of the distribution (error bars) of the signals were determined as well.

The mean H_{hf} values of the ^{55}Mn nuclei increase with increasing Fe content x, in agreement with the calculations. Remarkably, the general trend of the calculation, in particular if applying a constant term (dotted line with grey squares), is in line with experimental observation. The calculations underestimate the H_{hf} values by a constant shift of about 53 MHz (∼15%). This is a reasonable value, since there is always a deviation (up to 50%) for a hyperfine field obtained by a band-structure calculation.[43,44]

H. NMR linewidth

The linewidth of the quaternary compounds exhibits an apparent parabolic behavior (see Fig. 7). This behavior is related to higher shell effects which contribute to the behavior of the linewidth Γ[45] (see also Refs. 16 and 17) as a function of the Fe concentration x. The impact of higher shells on the linewidth can be demonstrated by comparing the linewidth in the ternary compound Co_2MnSi with one of the quaternary compounds, such as, e.g., $Co_2Mn_{0.9}Fe_{0.1}Si$. The first resonance line in $Co_2Mn_{0.9}Fe_{0.1}Si$ is attributed to Mn nuclei with no Fe atoms in the third shell, and therefore, this line also corresponds exactly to the third shell environment in unsubstituted Co_2MnSi. This is confirmed by the experimental observation that both lines exhibit the same resonance frequency (354.5 MHz). The linewidth in Co_2MnSi is very small (about 0.6 MHz), reflecting the fact that the ^{55}Mn nuclei have only one particular

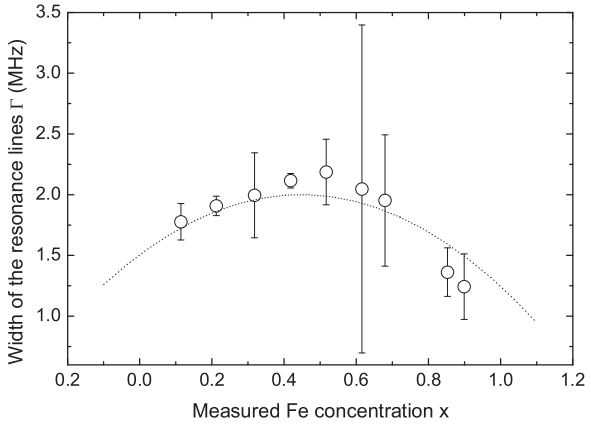

FIG. 7. Width of the Gaussian lines obtained from fits of the $Co_2Mn_{1-x}Fe_xSi$ substitutional series as a function of the measured Fe concentration x. Here, the black dotted line follows a phenomenological behavior described by $\Gamma = [x(1-x)\Sigma] + C$.

environment in the higher shells. The corresponding linewidth in $Co_2Mn_{0.9}Fe_{0.1}Si$ is 1.8 MHz, reflecting the distribution of hyperfine fields due to a random distribution of the Mn and Fe atoms in higher shells (but without Fe atoms in the third shell). Note, that a small contribution to the linewidth can also be given by small lattice distortions and a concomitant change of the quadrupole splitting. This linewidth behavior is also apparent from Fig. 3, revealing that the curves of the relative areas as a function of the number of Fe atoms in the third shell are both small for the Mn- and Fe-rich ones, but comparatively broad for compounds with medium Fe concentrations.

However, the linewidth seems to be modified by at least one additional factor, namely the subline spacing. The subline spacing is larger for the Mn-rich compounds and smaller for the Fe-rich ones (see above). This might also lead to a smaller spacing between adjacent resonance frequencies in higher shells for the Fe-rich compounds. Overall, the width depends on the substitution of Mn by Fe described by a binomial distribution, leading to the experimentally observed parabolic broadening with an additional modulation of the subline spacing. These contributions to the linewidth Γ are reasonably well described by an empirical model $\Gamma = [x(1-x)\Sigma] + C$ with $C = 1.34$ MHz, with x the Fe concentration, and Σ the subline spacing of the corresponding compound. The deviations between the experimental data and the model observed in case of the Fe-rich compounds with $x = 0.8$ and 0.9 may be attributed to the observation that Mn shows a small tendency to separate in Co_2FeSi, leading to a nonhomogenous distribution of Mn in the very Fe-rich compounds (see also discussion above).

III. SUMMARY

The local environment of the complete $Co_2Mn_{1-x}Fe_xSi$ substitutional series was investigated by means of ^{55}Mn NMR spectroscopy. Using the NMR technique, it was confirmed that the origin of the line splitting is a random distribution of Mn and Fe in third and higher shells of the ^{55}Mn nuclei. The systematic analysis of the complete substitutional series $Co_2Mn_{1-x}Fe_xSi$ showed that the spacing between adjacent resonance lines is approximately constant within a compound, and decreases with increasing overall Fe concentration x. This observation supports the model that neighboring Fe in the third nearest-neighbor shell contribute to a transferred hyperfine field. The decrease of the subline spacing was related to the gradual filling of different bands with different s character and different hybridization with increasing Fe content x. The change in the density of states is also contributing to the decrease in the resonance frequencies for the Fe-rich environments, and to the shift of the whole spectrum, revealing a "bending" of the hyperfine field dependence on x, present in this compound. The observed bending may also reflect the transition from a more localized (Mn-rich compositions) to a more itinerant (Fe-rich compositions) character.

All results, as presented in the previous sections, unambiguously confirm the $L2_1$ structure with a random distribution of Mn and Fe on the 4b Wyckoff position for the complete substitutional series. Band-structure calculations discussed in Ref. 1 by Balke *et al*. predict a very stable half metallicity of the compounds with $x \approx 0.5$. These calculations were performed using a supercell with a preferential distribution of Fe and Mn. Thus, it might be quite relevant to recalculate the band structure of $Co_2Mn_{1-x}Fe_xSi$ including the experimentally verified random distribution of Mn and Fe, and to check whether the minority band gap and the half metallicity is conserved. The high structural order of all members of the substitutional series, demonstrated by the ^{55}Mn NMR results, is one important ingredient for the possibility to observe the half-metallic character and the high degree in spin polarization of $Co_2Mn_{1-x}Fe_xSi$ and illustrates that in particular the $Co_2Mn_{1-x}Fe_xSi$ compounds with $x \approx 0.5$ may be ideal candidates for spintronic applications.

ACKNOWLEDGMENTS

S.W. gratefully acknowledges funding by Deutsche Forschungsgemeinschaft DFG, project WU 595/1-1 and project WU 595/3-1 (Emmy Noether program). We thank G. H. Fecher for allowing us to use his calculational data and for the very fruitful discussion of the results. We also thank C. Felser for discussions. We acknowledge M. E. Belesi and S. Rodan for help in finalizing of the manuscript. This work has been supported in part by a grant from by the Ministry of Sciences and Higher Education of Poland under Research Project No. 4531/B/T02/2010/38 for the years 2010–2013.

*s.wurmehl@ifw-dresden.de

[1] B. Balke, G. H. Fecher, H. C. Kandpal, C. Felser, K. Kobayashi, E. Ikenaga, J.-J. Kim, and S. Ueda, Phys. Rev. B **74**, 104405 (2006).

[2] G. H. Fecher and C. Felser, J. Phys. D: Appl. Phys. **40**, 1582 (2007).

[3] N. Tezuka, N. Ikeda, F. Mitsuhashi, and S. Sugimoto, Appl. Phys. Lett. **94**, 162504 (2009).

[4]R. Shan, H. Sukegawa, W. H. Wang, M. Kodzuka, T. Furubayashi, T. Ohkubo, S. Mitani, K. Inomata, and K. Hono, Phys. Rev. Lett. **102**, 246601 (2009).
[5]M. Kallmayer, H. J. Elmers, B. Balke, S. Wurmehl, F. Emmerling, G. H. Fecher, and C. Felser, J. Phys. D: Appl. Phys. **39**, 786 (2006).
[6]Fr. Heusler, Verh. Dtsch. Phys. Ges. **12**, 219 (1903).
[7]G. E. Bacon and J. S. Plant, J. Phys. F: Metal Phys. **1**, 524 (1971).
[8]S. Wurmehl, G. H. Fecher, K. Kroth, F. Kronast, H. A. Dürr, Y. Takeda, Y. Saitoh, K. Kobayashi, H.-J. Lin, and G. Schönhense, J. Phys. D: Appl. Phys. **39**, 803 (2006).
[9]S. Picozzi, A. Continenza, and A. J. Freeman, Phys. Rev. B **69**, 094423 (2004).
[10]Y. Miura, K. Nagao, and M. Shirai, Phys. Rev. B **69**, 144413 (2004).
[11]Y. Miura, K. Nagao, and M. Shirai, J. Appl. Phys. **95**, 7225 (2004).
[12]G. H. Fecher, H. C. Kandpal, S. Wurmehl, J. Morais, H.-J. Lin, H.-J. Elmers, and G. Schönhense, J. Phys.: Condens. Matter **17**, 7237 (2005).
[13]S. Wurmehl, G. H. Fecher, H. C. Kandpal, V. Ksenofontov, C. Felser, H.-J. Lin, and J. Morais, Phys. Rev. B **72**, 184434 (2005).
[14]B. Balke, S. Wurmehl, G. H. Fecher, C. Felser, Maria C. M. Alves, F. Bernardi, and J. Morais, Appl. Phys. Lett. **90**, 172501 (2007).
[15]S. Wurmehl, J. T. Kohlhepp, H. J. M. Swagten, B. Koopmans, M. Wojcik, B. Balke, C. G. H. Blum, V. Ksenofontov, G. H. Fecher, and C. Felser, Appl. Phys. Lett. **91**, 052506 (2007).
[16]S. Wurmehl, J. T. Kohlhepp, H. J. M. Swagten, B. Koopmans, M. Wojcik, B. Balke, C. G. H. Blum, V. Ksenofontov, G. H. Fecher, and C. Felser, J. Appl. Phys. **103**, 07D706 (2008).
[17]S. Wurmehl, J. T. Kohlhepp, H. J. M. Swagten, B. Koopmans, C. G. F. Blum, V. Ksenofontov, H. Schneider, G. Jakob, D. Ebke, and G. Reiss, J. Phys. D: Appl. Phys. **42**, 084017 (2009).
[18]J. Schaf, I. A. Campbell, K. Le Dang, and P. Veillet, J. Magn. Magn. Mater. **36**, 310 (1983).
[19]W. Van Roy, M. Wojcik, E. Jedryka, S. Nadolski, D. Jalabert, B. Brijs, G. Borghs, and J. De Boeck, Appl. Phys. Lett. **83**, 4214 (2003).
[20]H. Wieldraaijer, W. J. M. de Jonge, and J. T. Kohlhepp, Phys. Rev. B **72**, 155409 (2005).
[21]S. Wurmehl, P. J. Jacobs, J. T. Kohlhepp, H. J. M. Swagten, B. Koopmans, S. Maat, M. J. Carey, and J. R. Childress, Appl. Phys. Lett. **98**, 012506 (2011).
[22]See Supplemental Material at http://link.aps.org/supplemental/10.1103/PhysRevB.88.134424 for experimental details (Sec. A).
[23]M. Wójcik, E. Jedryka, H. Sukegawa, T. Nakatani, and K. Inomata, Phys. Rev. B **85**, 100401 (2012).
[24]S. Nadolski, M. Wojcik, E. Jedryka, and K. Nesteruk, J. Magn. Magn. Mater. **140–141**, 2187 (1995).
[25]A. J. Freeman and R. E. Watson, Phys. Rev. Lett. **5**, 498 (1960).
[26]Le Dang Khoi, P. Veillet, and I. A. Campell, J. Phys. F: Metal Phys. **8**, 1811 (1978).
[27]S. Wurmehl and J. T. Kohlhepp, J. Phys. D: Appl. Phys. **41**, 173002 (2008).
[28]P. Panissod, in *NATO ASI Series High Tech*, edited by V. G. Baryakhtar, P. E. Wigen, and N. A. Lesnik (Kluwer Academic, Dordrecht, 1997), Vol. 48, p. 225.
[29]P. C. Riedi, T. Thomson, and G. J. Tomka, in *Handbook of Magnetic Materials*, edited by K. H. J. Buschow (North-Holland, Amsterdam, 1999), Vol. 12, p. 97.
[30]K. Inomata, S. Okamura, A. Miyazaki, M. Kikuchi, N. Tezuka, M. Wojcik, and E. Jedryka, J. Phys. D: Appl. Phys. **39**, 816 (2006).
[31]S. Wurmehl, J. T. Kohlhepp, H. J. M. Swagten, and B. Koopmans, J. Phys. D: Appl. Phys. **41**, 115007 (2008).
[32]K. Inomata, M. Wojcik, E. Jedryka, N. Ikeda, and N. Tezuka, Phys. Rev. B **77**, 214425 (2008).
[33]V. Jung, G. H. Fecher, B. Balke, V. Ksenofontov, and C. Felser, J. Phys. D: Appl. Phys. **42**, 084007 (2009).
[34]V. Niculescu, T. J. Burch, K. Raj, and J. I. Budnick, J. Magn. Magn. Mater. **5**, 60 (1977).
[35]V. A. Niculescu, W. A. Hines, J. I. Budnick, J. Perkins, G. C. Papaefthymiou, and T. J. Burch, Phys. Rev. B **23**, 2388 (1981).
[36]See Supplemental Material at http://link.aps.org/supplemental/10.1103/PhysRevB.88.134424 for a description of the changes in the third shells surrounding due to Y by Y' substitution in X_2YZ (Sec. B).
[37]See Supplemental Material at http://link.aps.org/supplemental/10.1103/PhysRevB.88.134424 for the comparison of the measured Fe concentration x with the nominal (Sec. C).
[38]T. Nakamichi and C. V. Stager, J. Magn. Magn. Mater. **31–34**, 85 (1983).
[39]J. Kübler, A. R. William, and C. B. Sommers, Phys. Rev. B **28**, 1745 (1983).
[40]K. H. J. Buschow and P. G. van Engen, J. Magn. Magn. Mater. **25**, 90 (1981).
[41]See Supplemental Material at http://link.aps.org/supplemental/10.1103/PhysRevB.88.134424 for details on the dilute limit (Sec. D).
[42]M. Kawakami, M. Nagahama, and S. Satohira, J. Phys. Soc. Jpn. **59**, 4466 (1990).
[43]R. Kirsch, M. J. Prandolini, O. Beutler, W. D. Brewer, M. Gruyters, J. Kapoor, D. Riegel, H. Ebert, and S. Frota-Pessôa, Europhys. Lett. **59**, 430 (2002).
[44]M. Battocletti and H. Ebert, Phys. Rev. B **64**, 094417 (2001).
[45]P. Panissod, J. P. Jay, C. Meny, M. Wojcik, and E. Jedryka, Hyperfine Interact. **97/98**, 75 (1996).